231997

UCRL-JC-124897
PREPRINT

Modeling for Deformable Mirrors and the Adaptive Optics Optimization Program

M. A. Henesian, S. W. Haney,
M. Thomas, and J. B. Trenholme

This paper was prepared for submittal to the
2nd Annual International Conference on Solid-State Lasers
for Applications to Inertial Confinement Fusion
Paris, France
October 22-25, 1996

March 18, 1997

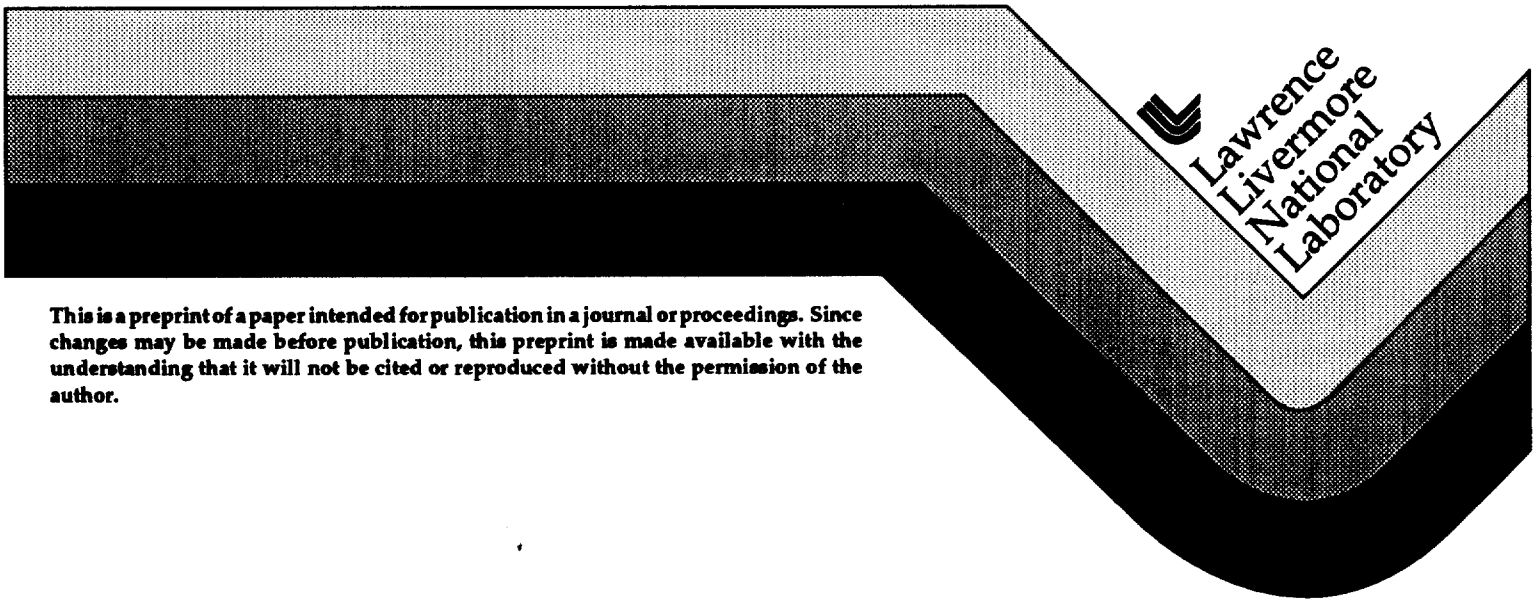

Modeling for Deformable Mirrors and the Adaptive Optics Optimization Program

M. A. Henesian, S. W. Haney, M. Thomas[†], and J. B. Trenholme

Lawrence Livermore National Laboratory
P. O. Box 808, L-490
Livermore, CA 94551-9900

[†]MIT Plasma Fusion Center
167 Albany Street
Cambridge, MA 02134

ABSTRACT

We discuss aspects of adaptive optics optimization for large fusion laser systems such as the 192-arm National Ignition Facility (NIF) at Lawrence Livermore National Laboratory (LLNL). By way of example we considered the discrete actuator deformable mirror and Hartmann sensor system used on the Beamlet laser. Beamlet is a single-aperture prototype of the 11-0-5 slab amplifier design for NIF, and so we expect similar optical distortion levels and deformable mirror correction requirements. We are now in the process of developing a numerically efficient object oriented C++ language implementation of our adaptive optics and wavefront sensor code, but this code is not yet operational. The results shown below are based instead on the prototype algorithms, coded-up in an interpreted array processing computer language.

Keywords: adaptive optics code, deformable mirrors, Beamlet laser, C++ computer language

2. INTRODUCTION

Coherent optical adaptive techniques (COAT) utilizing deformable or so called "rubber" mirrors played a major role the 1970's and early 80's in increasing laser fluence from high energy lasers on distant targets, obscured by refractive index distortions from atmospheric turbulence, thermal heating of the atmosphere by the laser beam, as well as source related problems such as laser amplifier medium distortions, optical transport system aberrations, and pointing and tracking errors.[1] We have many of the same problems, of course, in directing high power laser beams onto sub-millimeter sized targets intended for inertial confinement fusion (ICF) research, and must deal with tens to hundreds of laser arms, large optical components and long beamlines. Adaptive optics research, particularly from the late 1980's onward, has had a major impact on improving the focal plane image quality of astronomical systems with apertures typically exceeding 1-meter. Today some 20 observatories utilize laser generated "guide stars" or "beacons" and adaptive optics control systems. Laser generated Rayleigh scatter in the lower atmosphere (10-20 km), or resonant fluorescence from Na in the upper atmosphere (90-100 km) create the "guide star". The "guide star" is imaged through the telescope optics onto a Shack-

Hartmann wavefront sensor. The wavefront gradient data from the sensor is used in an active control loop to drive the actuators on the deformable mirror in the telescope's secondary optical train to increase the focusability of the system. If the "guide star" is in the same (or nearly the same) field of view as the astronomical object, then a highly corrected focal plane can be achieved. Astronomy-based deformable mirrors with tens to several hundred actuating elements have been successfully fielded.[2]

For much the same reasons, designers of large aperture laser systems for ICF consider adaptive optics wavefront correction of utmost importance to maintain high target irradiance levels and accurate target pointing. The adaptive optics requirements for the 192-arm NIF at LLNL have been detailed in the conceptual design report.[3] A 70 x 70 mm aperture deformable mirror has been successfully implemented on the Beamlet system at LLNL and is mated to a Shack-Hartmann sensor with 77 lens elements. The Beamlet deformable mirror uses a highly-reflective dielectric coating on a continuous glass substrate, on the back of which is attached the 39 PMN (electrostrictive lead-manganese-niobate ceramic) actuators in a hexagonal arrangement.[4] The 60 x 60 mm central region of the mirror controls the 34 x 34 cm Beamlet aperture. The 70-mm size deformable mirror is located in the path ahead of the optics that inject the beam into the 4-pass amplifier cavity. Beamlet uses both an input and output Hartmann sensor, and a diffraction limited CW reference beam in conjunction with the input Hartmann sensor to perform the mirror calibration. A paper by J. T. Salmon and coworkers describes the Livermore system.[5] This system has achieved a focusability as measured by the Strehl ratio[6] of greater that 0.5 at moderate (1 TW) system powers, in an otherwise "cold" system, by pre-correcting for the prompt flashlamp-induced thermal distortion in the slab amplifiers. Recently, closed-loop deformable mirror correction has been extended to 1-second ahead of a system shot, thus allowing substantial beam focusability improvement in a "hot" system; that is, a system with thermal distortions in the heated air columns and residual thermal distortions in the slab amplifiers.[7] Work is ongoing to quantify the improvements.

A 40 x 40 cm aperture deformable mirror (clear aperture of 36.5 x 36.5 cm) with 39 actuators is now under construction at LLNL for testing on Beamlet, and will demonstrate adaptive optics control from within the main multi-pass cavity, at full beam size, rather than in the front-end optics as is now implemented on Beamlet. This 40-cm mirror will replace one of the cavity mirrors. Since this mirror will see two bounces prior to laser pulse switch-out from the main cavity, a higher level of peak-to-valley wavefront correction can be applied, up to 20 waves peak-to-valley[8], thus potentially allowing a faster shot rate or reduced amplifier cooling. With a full scale mirror, a higher density and/or nonuniform placement of actuators might be attempted to optimize the mirror design against specific aberrations that we expect. Also, a large mirror might be used in conjunction with a specialized small mirror or an advanced spatial phase modulation system.[9] Adaptive optics are also being investigated at Osaka University[10] for use on Gekko XII system, and by Commissariat a L'Energie Atomique (CEA) for the 240-arm Laser Megajoule (LMJ) system. The Osaka mirror design has been demonstrated at the 40-cm diameter with 37 mechanical actuators for use with the 32-cm diameter Gekko XII beam.

3. MODELING RESULTS

Optimization of a deformable mirror design involves significant variation of mirror parameters such as the spacing between actuators, actuator density in the active beam area, the shape of the actuator influence profiles, and the degree of actuator cross-coupling. Of consideration to the mechanical designer of the mirror, but not to us, are such things as substrate stiffness, actuator stiffness, actuator force requirements, and actuator mechanical efficiency, which is the ratio of mechanical surface deformation to actuator displacement. These mechanical parameters determine the surface deformation profiles, the actuator centers of influence, and edge-distortion effects. In modeling we will always assume that the accumulated surface deformation profile for the mirror is the linear superposition of profiles from each actuator, acting independently. Thus from actuator force and linearity requirements, the surface deformations cannot be more than 5 or so waves. The mirror performance at a fixed design varies strongly with the type of wavefront aberration that we are attempting to correct. We will illustrate this below, specifically with the 39-actuator Beamlet mirror design. We note that other lower and higher density designs utilizing a hexagonal arrangement of actuators and Hartmann lenses have been considered. Figure 1 illustrates three such designs using 23, 39, or 59 actuators with corresponding 59, 77, or 127 wavefront sensor locations. If M equals the number of actuators on the top row and N the number in the next row (N = M - 1), say M = 5 and N = 4, then the number of actuator rows is N + M + 4 = 13, and columns is N + M = 9. The total actuator count is (N+2)N + (M+2)M = 59, and the minimum number of Hartmann sensor locations is $6M^2$ - 4M - 3 = 127. The circles represent the sensor locations and the + signs label the centers of actuator influence. Note that the outer rows and columns of actuators are displaced outwardly (from their mechanical centers - not shown). Detailed measurements on the Beamlet mirror show that the influence function shapes resemble elliptical Gaussian profiles for the outer actuators (ellipticity ~ 120%) rather than the very nearly circular Gaussian profiles for central actuators. On the Beamlet mirror, the actuator cross coupling for central actuators is 10 mm half-width (at 1/e) at a spacing of 11.5 mm. With a Gaussian influence shape, the coupling is therefore 27 %. The optical magnification following the Beamlet mirror is 5.673, so the actuator spacing projected to the full beam is 6.52-cm. Assuming that the mirror can correct a spatial sinusoidal ripple with a period twice the actuator spacing, the 39-actuator mirror would effect the far field irradiance out to 8.1 μradians. Simulations indicate that when the mirror is required to correct high wavefront gradients for large thermal distortions, the far field beyond 8.1 μradians can be significantly affected. Therefore, a simplified spatial frequency domain modeling approach for the mirror in a real system is insufficient.

Coworkers at LLNL have identified many of the sources of wavefront distortion on Beamlet.[5] Long spatial scale (>10 cm) static aberrations from spatial filter lenses and amplifier disks give 2 to 2.5 waves peak-to-valley error at the output diagnostics plane. Small scale finishing errors are a few tenths of a wave. In a "cold" system, the prompt flashlamp-induced thermal distortion in the amplifier disks is approximately 2-waves in after (4-passes at 11 slabs/pass + 5 booster slabs) = 49 amplifier slabs. Once the system has been "fired", nonuniform cooling increases the peak-to-valley distortion (mostly long-scale) from 2.5 to 5 waves, depending on cool-down time.

At four hours the aberration resembles 2-waves of cylinder in the vertical direction and about 1 wave of opposite cylinder distortion along the horizontal. The thermal "turbulence" effects in the air columns result in up to 0.5 waves peak-to-valley fluctuation in a "cold" system, and up to 1.0 wave in a "hot" system. The spatial scale for these air column effects is reported to be at 3-cm and longer. Figures 2, 3, and 4 illustrate the three aberration types that we used in the modeling. The prompt pump-induced distortion in the amplifier slabs is shown in the left picture in Fig. 2. Static medium scale aberrations are also present from the spatial filter lenses, in addition to the slabs. The left picture in Fig. 3 shows the wavefront on a second system shot, with added thermal distortion following a three to four-hour cool-down from a previous shot. The peak-to-valley distortion has increases from 1.77 waves to 3.00 waves. The r.m.s. value went from 0.371 to 0.601 waves, and the Strehl ratio dropped from 0.126 to 0.015. When the effects of air column "turbulence" are added, we obtain the wavefront shown in Fig. 4. This wavefront includes ~1 wave additional peak-to-valley distortion at a correlation radius of 5-cm. This aberration was randomly generated using a Gaussian random aberration model scaled to a peak-to-valley of 0.316-waves, applied at the entrance and exit planes of the 4-pass cavity 11-slab amplifier section, and the single-pass 5-slab booster amplifier section. The total system peak-to-valley error increased to 4.64 waves, the r.m.s. error increased to 0.989 waves, and the Strehl ratio dropped to a rather meaningless 2.6×10^{-4}. Note that this random aberration was "cooked" up in the Beamlet system model, but is based on overall peak-to-valley measurements using the output Hartmann sensor. It does not represent any specific data. The prompt pump-induced distortion and thermal distortion from previous slab heating are based on low resolution system measurements.[5]

In the adaptive optics code we simulate the mirror calibration procedure.[4] We push each actuator by a fixed amount (1-μm), and calculate the distortion of the mirror surface above the center of influence of the actuator, and the wavefront gradients of a reference beam at the Hartmann lens locations using a far field algorithm and gray-scale centroiding (with thresholding at 1% for numerical stability). To build the "reconstruction" matrix[9] for the control loop, we invert the 39 by 154 matrix of Hartmann sensor wavefront gradient values using the singular value decomposition method of least-squares-estimation. Since the wavefront gradient has x-and y-components, there are 154 gradient values - double the number of lenses. The output field for laser system simulation with a "flat" mirror is read into the Hartmann sensor code which returns the 154 element array of wavefront gradient values. Matrix multiplying the gradient array by the reconstruction matrix returns the amplitude or "push" on each of the 39 actuators. Influence function specifications for the Beamlet mirror, or scaled from the Beamlet mirror, are then used to re-create the mirror surface. Changing the sign of the actuator amplitudes amounts to generation of the "phase-conjugate" surface required for pre-correction. Mirror location, as well as single or double-bounce considerations, may require a scaling and/or inversion correction to the mirror surface. By scaling the influence function radius and considering various influence function shapes, such as super or sub-Gaussian shapes, for example, we can examine the performance of a given mirror design.

Examples of adaptive optics corrections for the three target aberration types discussed above are also shown in Figs 2 to 4. The system simulation with a "flat" mirror is performed first so that the wavefront will sample the static, pump-induced, and thermal aberrations built in the system model. This uncorrected wavefront is shown in the left-most picture, as explained above. The mirror pre-correction shapes are calculated from the field at the output relay plane (also the output Hartmann sensor plane) and then used in a second run with pre-corrections applied at the small mirror location. The mirror pre-correction shapes, as applied to the wavefront, are shown in the center pictures. The right-most picture is the output wavefront with the adaptive optics corrections. Starting from a "cold" system, the pre-correction increases the Strehl ratio to 0.668, the peak-to-valley is reduced to 1.025, and the r.m.s. error is reduced to 0.097, as shown in Fig. 2. Adding longer scale thermal aberrations to a "hot" system appears not to stress the 39-actuator mirror, as shown in Fig. 3. The Strehl ratio is increased to 0.690, the peak-to-valley reduced to 1.096 waves, and r.m.s. error reduced to 0.095 waves. When Gaussian random thermal fluctuations are introduced at a scale below the actuator spacing as shown in Fig. 4, the 39-actuator mirror has difficulty but still can achieve a Strehl ratio of 0.109. The large peak-to-valley variaton of 4.64 waves is reduced to 1.82 waves and the r.m.s. error goes to 0.248 waves. The mirror in this case must have a stroke of over 5 waves to control the far field irradiance. Far field irradiance images for 3.8 TW simulations are shown in Figs. 5 and 6. The left image is the simulated irradiance with the "flat" mirror, the right shows the irradiance with the adaptive optics. In a "cold" system, with the current Beamlet model, we predict that the 80% enclosed power radius can be reduced from 20.8 to 14.7 μradians at 3.8 TW. In a "hot" system with serious thermal distortion, the 80% radius might only be reduced from 24.8 to 19.8 μradians. At power levels below 1 TW, we predict that the 14.7 could go down to 8.6 μradians in a "cold" system, and from 19.8 down to 15.2 μradians in a "hot" system. While these images have a striking resemblance to real data and are in good agreement with parts of the data set, remember that they are only simulations, dependent strongly on various assumptions and short-comings of any system model. We are continuing to investigate the laser modeling issues and whether higher density adaptive optics can provide a cost/performance benefit, considering the focusability requirements for the various NIF target missions.

4. CONCLUSION

We mentioned in the abstract that we are working on a C++ version of our adaptive optics modeling code. Our laser system propagation and simulation codes at LLNL are also being rewritten in C++. We are doing this to exploit modern programming design techniques such as abstraction, inheritance, and encapsulation. Also, recent advances in compiler technology and C++ class design, particularly the use of expression templates, allows scientific C++ to run as fast as FORTRAN.[11] Extensive use of vector and array classes allow scientists to translate physical models and mathematical expressions into readable, maintainable, and fast code. In addition, we believe that our C++ code will run efficiently in a parallel machine architecture with multi-processors and/or on multiple machines, thus providing the computational performance to allow intelligent optimization over a wide range of laser system and deformable mirror design parameters.

5. ACKNOWLEDGMENTS

We particularly wish to thanks our collegues at LLNL involved with deformable mirror engineering for Beamlet, NIF and the Beamlet laser science measurements, as well as other members of the Laser Modeling and Optimization group. Work performed under the auspices of the U.S. Department of Energy by Lawrence Livermore National Laboratory under Contract W-7405-Eng-48

6. REFERENCES

1. J. E. Pearson, R. H. Freeman, and H. C. Reynolds, Jr., "Adaptive Optical Techniques for Wave-Front Correction," Chapter 8, in *Applied Optics and Optical Engineering*, Vol. VII, ed. by R. R. Shannon and J. C. Wyant, Academic Press, c. 1979.

2. L. A. Thompson, "Adaptive Optics in Astronomy," *Physics Today*, December 1994, pp.24 31, 1994.

3. *National Ignition Facility Conceptual Design Report, Volume 3: Conceptual Design*, pp. 290-315, UCRL-PROP-117093, Vol. 3, NIF-LLNL-94-113, Livermore, CA (1994).

4. J. T. Salmon, J. W. Bergum, M. W. Kartz, R. W. Presta, and C. D. Swift, "Wavefront correction system based on an equilateral triangular arrangement of actuators," in *Active and Adaptive Optical Components and Systems II*, SPIE Proceedings 1920, 20 (1993).

5. J. T. Salmon, E. S. Bliss, J. L. Byrd, M. Feldman, M. A. Kartz, J. S. Toeppen, B. VanWonterghem, and S. E. Winters, "An adaptive optics system for solid-state laser systems used in inertial confinement fusion", in *First Annual International Conference on Solid State Lasers for Application to Inertial Confinement Fusion*, SPIE Proceedings 2633, pp. 105-113 (1995).

6. Our definition of Strehl ratio is the peak far field irradiance of the sampled beam divided by the peak far field irradiance of the same beam with a flat wavefront. For small aberrations as measured by the r.m.s. wavefront error, denoted s in units of waves, the Strehl ratio is approximately $\exp(-4\pi^2 s^2)$. A more rigorous derivation based on the Fraunhofer formula is $| \acute{U}da\, A_0(x,y) \exp(i2pf(x,y))|^2 / | \acute{U}da A_0(x,y)|^2$, where $A_0(x,y)$ is the spatial envelope of the electric field amplitude and f(x,y) is the wavefront aberration in waves.

7. M. Kartz, T. Salmon, E. Bliss, R. Hartley, W. Behrendt, G. Pollack, A. Hines, B. VanWonterghem, S. Winters, and R. Zacharias, "Wavefront correction for static and dynamic aberrations to within 1 second of the system shot in the NIF Beamlet demonstration facility," presented to *the Second Annual International Conference on Solid State Lasers for Application to Inertial Confinement Fusion*, October 22-25, 1996, Paris, France.

8. S. Winters, R. Zacharias, and E. Bliss, LLNL, internal memorandum, January 1997.

9. J.C. Chanteloup, B. Loiseaux, J.P. Huignard, H. Baldis, "Wave front detection and correction for ultra-intense laser systems," presented to the *Second Annual International Conference on Solid State Lasers for Application to Inertial Confinement Fusion*, October 22-25, 1996, Paris, France.

10. G. Y. Yoon, T. Jitsuno, M. Nakatsuka, and Y. Kato, "Development of a large aperture deformable mirror for the wavefront control", presented to the *Second Annual International Conference on Solid State Lasers for Application to Inertial Confinement Fusion*, October 22-25, 1996, Paris, France.

11. S. W. Haney, "Beating the abstraction penalty in C++ using expression templates," *Computers in Physics*, Vol. 10, No. 6, Nov/Dec 1996, pp.552-557 (1996).

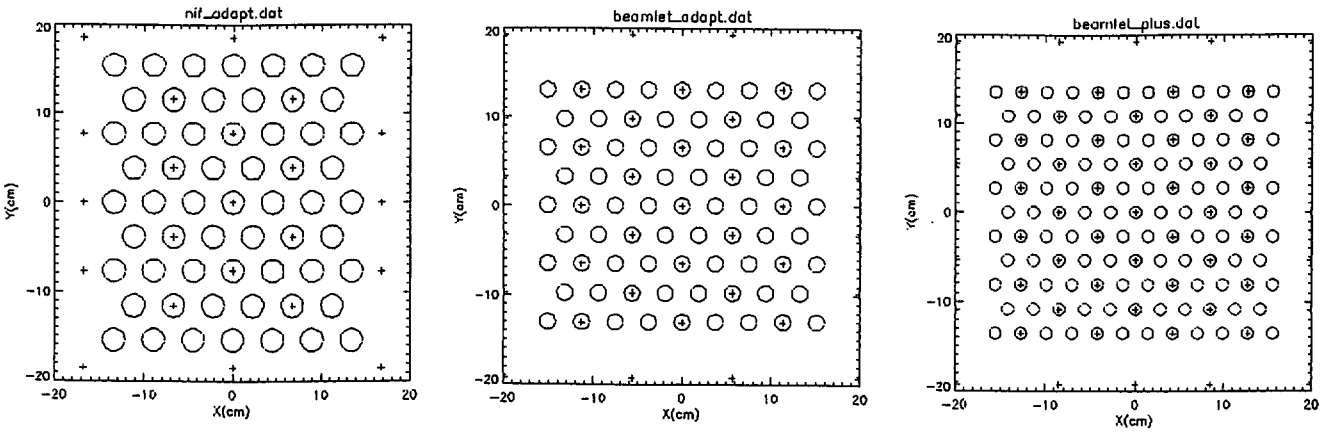

23 actuators/ 59 lenses: far field cut-off: 6.8 μradians

39 actuator/ 77 lenses: far field cut-off: 8.1 μradians

59 actuators/ 127 lenses: far field cut-off: 9.7 μradians

Figure 1. 23, 39, and 59 actuator deformable mirror designs, with 59, 77, and 127 element Shack-Hartmann sensor. Sensor locations are denoted by circle, actuator centers of influence denoted by + symbol. Beamlet design uses 39-actuators, shown in the middle picture. Note outward distortion of the centers of influence for the outer rows and columns of actuators.

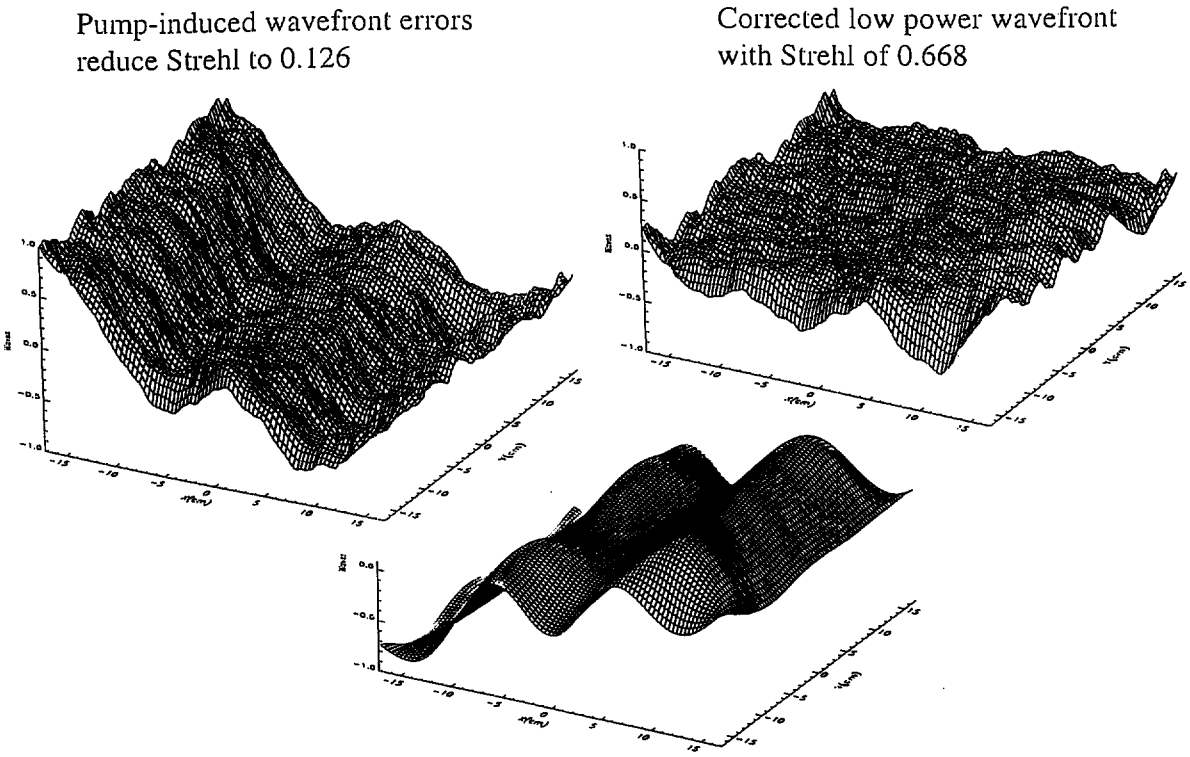

Figure 2. Simulated wavefronts for a "cold" Beamlet system at low power. Left- wavefront without pre-correction (1.77 waves P-V, 0.371 waves r.m.s., Strehl 0.126), Center- deformable mirror correction (1.69 waves), Right- pre-corrected wavefront (1.025 waves P-V, 0.097 waves r.m.s., Strehl 0.668).

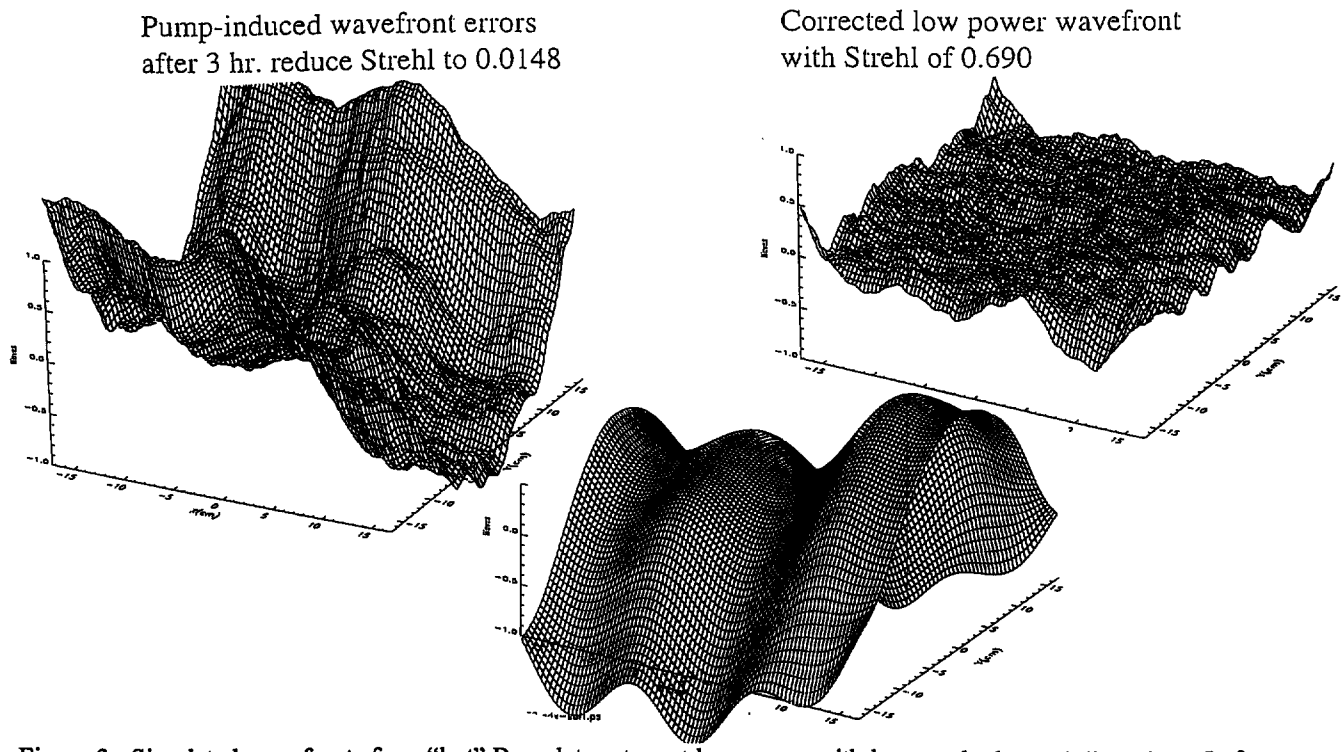

Figure 3. Simulated wavefronts for a "hot" Beamlet system at low power with long-scale thermal distortions. Left- without pre-corection (3.00 waves P-V, 0.601 waves r.m.s., Strehl 0.015), Center- deformable mirror correction (3.06 waves), Right- pre-corrected wavefront (1.096 waves P-V, 0.095 waves r.m.s., Strehl 0.690).

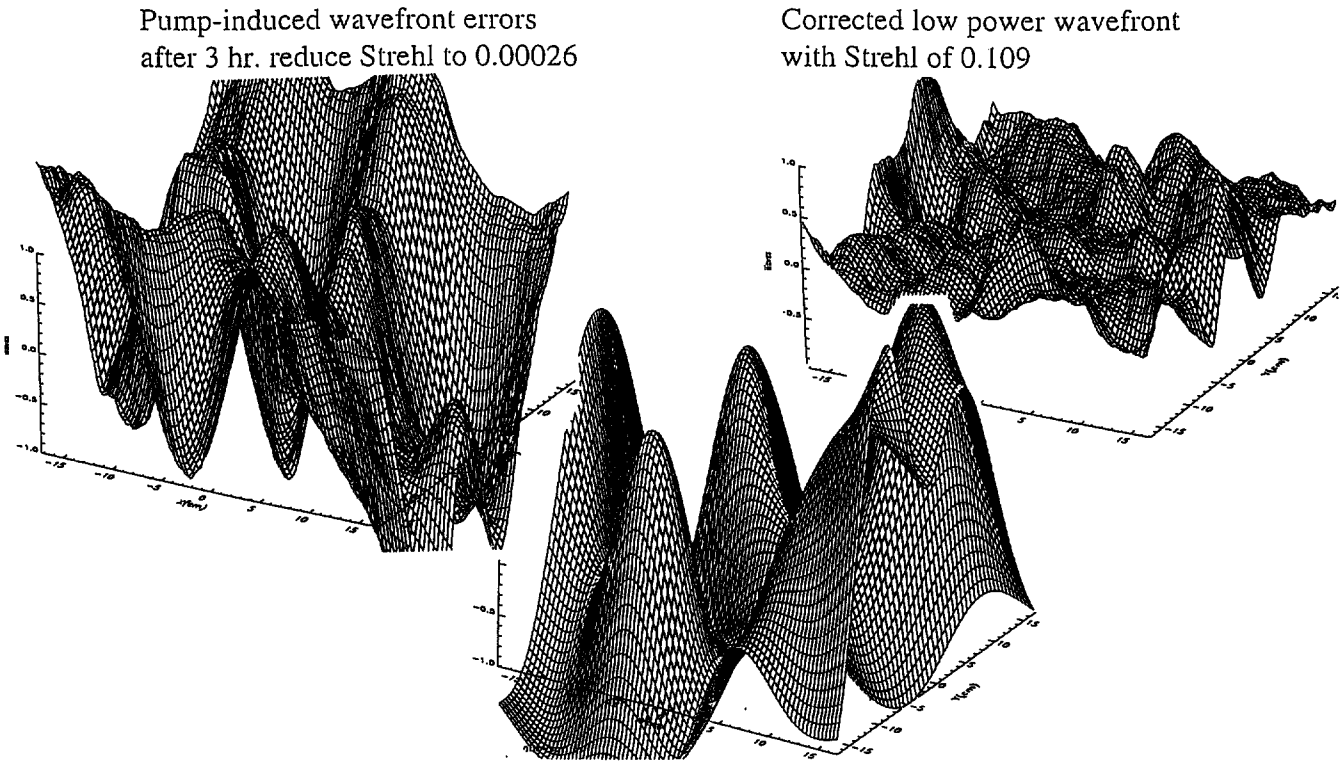

Figure 4. Simulated wavefronts for a "hot" Beamlet system at low power including air-path "turbulence". Left- without pre-correction (4.64 waves P-V, 0.989 waves r.m.s., Strehl 2.6 x 10^{-4}), Center- deformable mirror correction (5.08 waves), Right- pre-corrected wavefront (1.824 waves P-V, 0.248 waves r.m.s., Strehl 0.109).

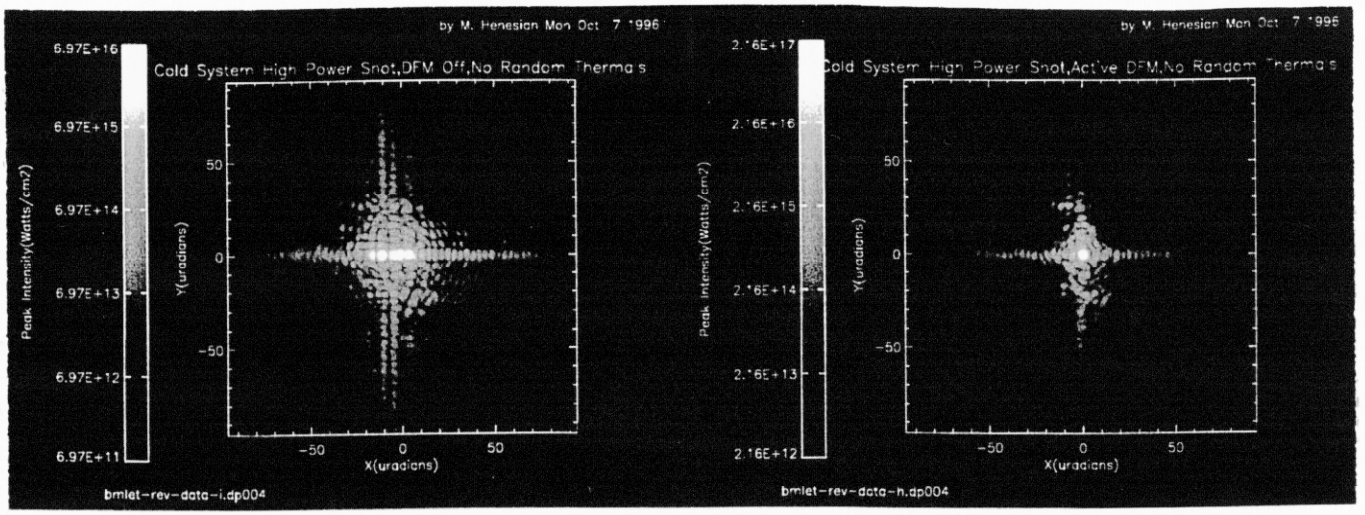

Deformable mirror inactive:
Strehl ratio: 0.069
80% power radius: 20.8 μR
95% power radius: 57.3 μR

Deformable mirror active:
Strehl ratio: 0.516
80% power radius: 14.7 μR
95% power radius: 59.6 μR

Figure 5. Simulated Beamlet far field irradiance for 3.8 TW power in a "cold" system (first shot of the day). Left- without adaptive optics correction, Right- with adaptive optics correction.

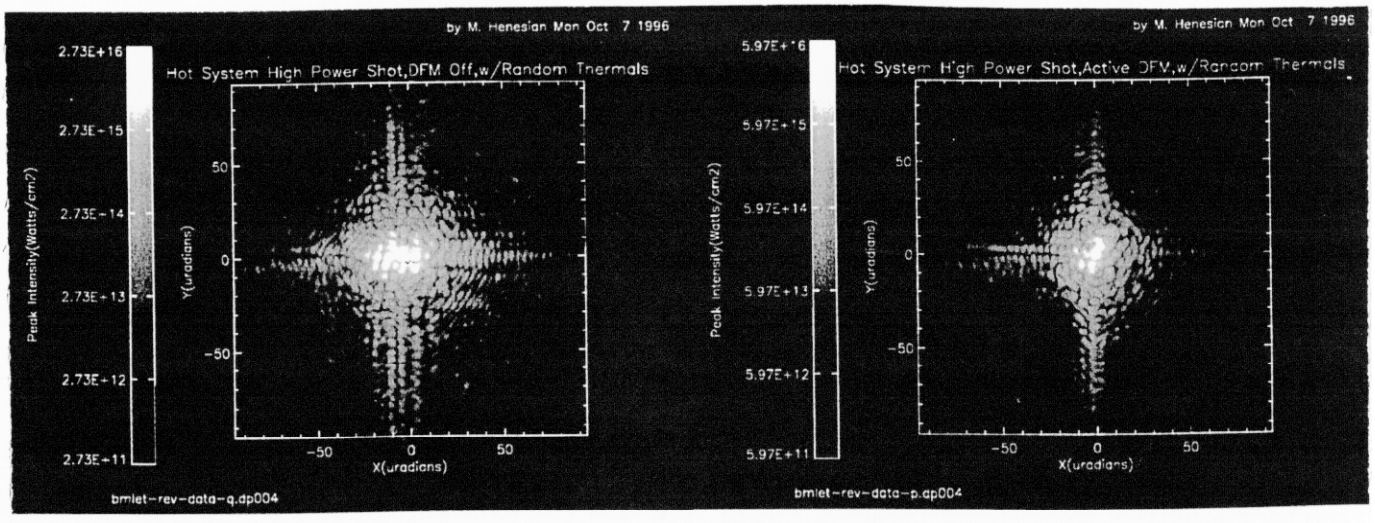

Deformable mirror inactive:
Strehl ratio: 0.018
80% power radius: 24.8 μR
95% power radius: 56.9 μR

Deformable mirror active:
Strehl ratio: 0.140
80% power radius: 19.8 μR
95% power radius: 58.7 μR

Figure 6. Simulated Beamlet far field irradiance for 3.8 TW power in a "hot" system (second shot of the day). Left- without adaptive optics correction, Right- with adaptive optics correction.

Technical Information Department • **Lawrence Livermore National Laboratory**
University of California • Livermore, California 94551